Low Temperature Physics/Fizika Nizkikh Temperatur, 2011, v. 37, Nos. 9/10, p. 959–969

Field-induced charge-density-wave transitions in the organic metal α-(BEDT-TTF)$_2$KHg(SCN)$_4$ under pressure

D. Andres, M.V. Kartsovnik, W. Biberacher, and K. Neumaier

Walther-Meissner-Institut, Bayerische Akademie der Wissenschaften, D-85748 Garching, Germany
E-mail: mark.kartsovnik@wmi.badw-muenchen.de

I. Sheikin

Laboratoire National des Champs Magnétiques Intenses, CNRS, 25 rue des Martyrs, B.P. 166, 38042 Grenoble Cedex 9, France

H. Müller

European Synchrotron Radiation Facility, F-38043 Grenoble, France

N.D. Kushch

Institute of Problems of Chemical Physics, Russian Academy of Sciences, 142432 Chernogolovka, Russia

Received May 10, 2011

Successive magnetic-field-induced charge-density-wave transitions in the layered molecular conductor α-(BEDT-TTF)$_2$KHg(SCN)$_4$ are studied in the hydrostatic pressure regime, in which the zero field charge-density-wave (CDW) state is completely suppressed. The orbital effect of the magnetic field is demonstrated to restore the density wave, while the orbital quantization induces transitions between different CDW states at changing the field strength. The latter appear as distinct anomalies in the magnetoresistance as a function of field. The interplay between the orbital and Pauli paramagnetic effects acting, respectively, to enhance and to suppress the CDW instability is particularly manifest in the angular dependence of the field-induced anomalies.

PACS: 71.45.Lr Charge-density-wave systems;
71.30.+h Metal-insulator transitions and other electronic transitions;
74.70.Kn Organic superconductors.

Keywords: organic conductor, electronic phase transitions, charge-density waves, field-induced charge-density waves, high pressure, magnetoresistance.

1. Introduction

Phase transitions in low-dimensional molecular conductors induced by a high magnetic field have been an intensively studied topic over the last two decades [1,2]. Among the most prominent examples are field-induced transitions to a spin-density-wave (SDW) state and the field-induced superconductivity. The former effect in strongly anisotropic quasi-one dimensional (Q1D) electron systems has its origin in an effective reduction of the dimensionality due to the orbital motion of charge carriers in magnetic field on open sheets of the Fermi surface [1–8], therefore being called orbital effect.

The layered organic metal α-(BEDT-TTF)$_2$KHg(SCN)$_4$ undergoes a phase transition into a charge-density-wave (CDW) state at $T_{CDW} \approx 8.5$ K at ambient pressure [9–13]. A Q1D electron band becomes gapped at the Fermi level, due to the so-called nesting of the Fermi surface, while the other, quasi-two-dimensional (Q2D) band still determines a metallic character of the system.

It has been found, that hydrostatic pressure deteriorates the nesting conditions and even leads to a complete suppression of the density wave at $P_0 \approx 2.5$ kbar [14,15]. The suppression is naturally explained by an increase in the dimensionality of the Q1D band with hydrostatic pressure which can be parametrized by an increasing ratio between the ef-

fective next-nearest and nearest interchain hopping integrals t_c'/t_c within the conducting *ac* plane. The complete suppression of the CDW state at P_0 has also been demonstrated to be directly reflected in a distinct impact on the superconducting state also existing in this compound [15].

Remarkably, it was shown [14] that this CDW state, akin to SDW, is sensitive to the orbital effect of magnetic field. By applying a field along the least conducting direction b^* (normal to conducting layers), it is possible that the imperfectly nested CDW state, at P = 1.5–2.5 kbar, even becomes stabilized before the suppression by the additional, Pauli paramagnetic effect sets in.

Furthermore, it was found that effects of orbital quantization take place in the present compound [16], causing the CDW wave vector to switch between quantized values at changing the magnetic field. Qualitatively, this effect emerges, if the nesting conditions of the Fermi surface become so bad that free carriers would start reappearing on the 1D sheets of the Fermi surface [17]. In the present case it was found that within the high field CDW_x state, existing above the paramagnetic limit [9–11], the Pauli effect is responsible for the unnesting [16,18]. This in turn suggests that worsening of the nesting conditions by hydrostatic pressure should also lead to a manifestation of orbital quantization effects [3,19,20].

The situation is fairly similar to the well-known SDW systems of the Bechgaard salts [1,2]. In those compounds, all carriers on the open sheets of the Fermi surface can be considered to be completely gapped below the critical pressure, while above they would become free, which eventually completely suppresses the density wave. In a magnetic field, best oriented along the least conducting direction, it is possible to again stabilize the density wave [3–7]. However, there will now be quantized values of the nesting vector most preferable, which gives rise to SDW subphases with field-dependent wave vectors. At low enough temperatures the SDW wave vector switches abruptly on going from one subphase to the next one, which causes a series of first order phase transitions at changing the magnetic field. Similar effects under hydrostatic pressure, namely field-induced CDW (FICDW) transitions, have already been proposed to occur in the organic CDW conductor α-(BEDT-TTF)$_2$KHg(SCN)$_4$ under pressure [14,21–23]. Some hints for the existence of FICDW transitions have recently been reported for other organic conductors (Per)$_2$Pt(mnt)$_2$ [24] and HMTSF-TCNQ [25]. However, the situation for the latter two compounds is rather intricate due to the more complex Q1D band structure and nontrivial magnetic properties.

Here we present direct experimental evidence that first order FICDW transitions indeed exist in the title compound under pressure. This is especially demonstrated by distinct hysteretic structures in the magnetoresistance, at sweeping the magnetic field up and down. In particular, it is shown that, by tilting the magnetic field towards the conducting plane, it is even possible to shift the onset temperature of the FICDW first order transitions to much higher values. This observation is shown to be in line with recent theoretical models of the FICDW phenomenon.

2. Experiment

Single crystals of α-(BEDT-TTF)$_2$KHg(SCN)$_4$ were obtained by electrooxidation of BEDT-TTF [26,27] and had the shape of distorted hexagonal platelets of typical dimensions ~ 0.7×0.3×0.1 mm. The interlayer resistance was measured by a standard four probe a.c. technique. The typical sample resistance at room temperature was ~ 10^3–10^4 Ω with contact resistances of ~ 30 Ω. Overheating of the samples was always checked to be negligible at applied currents of ~ 100 nA at 0.1 K.

To apply pressure, a big (20 mm diameter) and a small (10 mm diameter) BeCu clamp cell were used. The pressure at low temperatures was determined from the resistance of a calibrated manganin coil to accuracy better than ± 0.1 kbar. The temperature was monitored by the resistance of a RuO_x sensor below 0.3 K. The big cell was mounted on the cold finger of a home-made dilution refrigerator, the sample being oriented so that its conducting *ac* plane was perpendicular to the magnetic field generated by a superconducting magnet. In order to keep the lowest operating temperature of 100 mK, the rate of the field sweeps were chosen as small as 2 mT/s. At the lowest temperatures weak demagnetization effects of the pressure cell became significant and had to be taken into account at controlling the temperature. All in all, the lowest temperature could be kept constant during a field sweep up to 15 T to an accuracy of ≤ 10%.

Effects of field orientation were studied in the 28 T resistive magnet at the High Magnetic Field Laboratory (LNCMI) in Grenoble using the small pressure cell. The cell was mounted on a ^{3}He two-axes rotation insert. The absolute values of both angles determining the sample orientation could be measured to an accuracy better than 0.5°, and changed with the resolution better than 0.05°. Field sweeps at fixed field orientations were made at temperatures down to 0.4 K. The angle-dependent magnetoresistance at fixed field intensities was measured by sweeping the polar angle θ at different azimuthal angles φ. At reasonable sweep rates of ~ 0.1°/s the lowest achievable temperature was 0.7 K.

3. Re-entrant CDW state under pressure

The critical pressure P_0, at which the zero-field density-wave transition becomes fully suppressed has been determined as (2.5 ± 0.1) kbar [14,15]. Above P_0 we expect the CDW state only to become stabilized via the orbital effect of magnetic field. Figure 1 shows magnetic field sweeps up to 15 T with the field directed perpendicular to the conducting plane, at 100 mK for different pressures covering

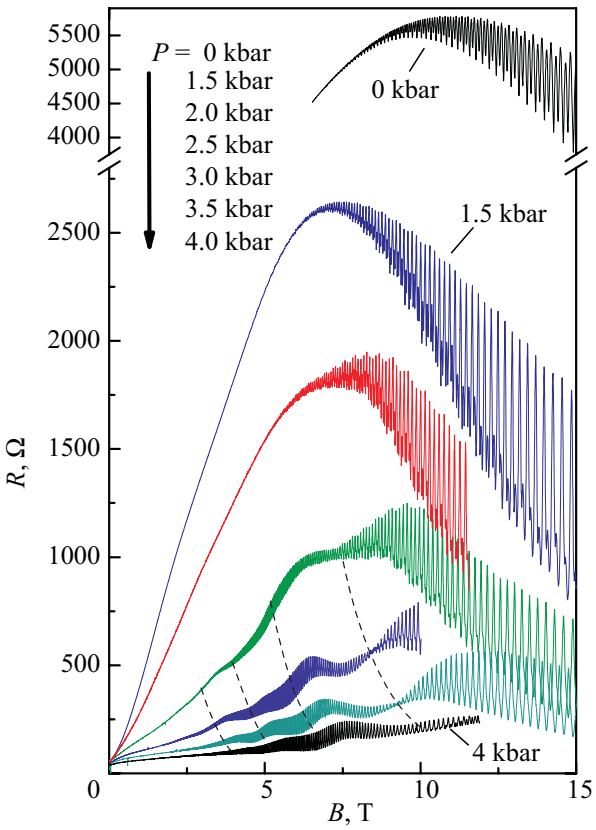

Fig. 1. Magnetoresistance at different pressures at 100 mK. Above $P_0 \approx 2.5$ kbar slow oscillations emerge in the magnetoresistance background. With increasing pressure these oscillations gradually shift to higher fields as indicated by dashed lines.

the whole pressure range investigated within this work. The data presented in Fig. 1 are obtained on one and the same sample and have been qualitatively reproduced on another one measured at the same time. Since the pressures were applied successively, i.e., without opening the clamp cell, the magnetic field orientation is exactly the same for each pressure.

One of the basic features of the ambient-pressure CDW state of the present compound is the strong magnetoresistance, $R(10\ \text{T})/R(0\ \text{T}) \sim 10^2$ at low T, most likely caused by a reconstruction of the closed orbits of the Q2D carriers in the presence of the CDW potential [28,29]. At ≈ 11 T the magnetoresistance has a maximum followed by a negative slope associated with a reentrance to the closed orbit topology due to magnetic breakdown [30] between the strongly warped open sheets of the Fermi surface. The latter also allows the fast Shubnikov–de Haas (SdH) oscillations at frequency $F_\alpha = 670$ T corresponding to the undisturbed Q2D band to appear. Moreover, it is known, that there is an anomalously strong second harmonic signal at $2F_\alpha$ as well as additional SdH frequencies at $F_\lambda = 170$ T and $F_\nu = F_\alpha + F_\lambda$, which only appear in the CDW state. The origin of these multiple frequencies is obviously related to the complex magnetic-breakdown network, although their detailed description is somewhat controversial [28,29,31–33].

Under pressure, the magnitude of the magnetoresistance in Fig. 1 becomes smaller. We attribute it to the gradual suppression of the CDW energy gap. Besides this, the curves show other pressure-induced changes, in particular on crossing the critical pressure P_0. Most significantly, at pressures $P \geq P_0$ slow oscillations emerge in the magnetoresistance background. At increasing pressure, these oscillations gradually move up in field, as visualized by the dashed lines in Fig. 1. The oscillation amplitude is maximum at 3–3.5 kbar and reduces at further increasing pressure. Remarkably, these slow oscillations occur exactly in the pressure range, in which FICDW transitions are expected, i.e. at $P \geq P_0$.

Another distinct change detected at driving pressure through the critical value is a sharp decrease of the minimum field required for observation of the fast SdH. While at $P < P_0$ these oscillations appear at rather high fields, ~7 T, shortly before the magnetoresistance background reaches the maximum, at $P > P_0$ we can clearly resolve them down to below 2 T. This is demonstrated in Fig. 2, in which the field sweeps around 2 T are shown in an enlarged scale at pressures above and below 2.5 kbar.

To better understand these changes at $P > P_0$, it is instructive to take a closer look at how the slow oscillations develop at lowering temperature. In Fig. 3 field sweeps taken at 3 kbar are shown for different temperatures. At 4.2 K the resistance increases rather moderately with field and no sign of any anomaly is seen. We, thus, consider the normal metallic state at this temperature to be present over the whole field range. At 2.5 K, a stronger enhancement of the magnetoresistance starting from ≈ 6 T indicates the reentrance into the CDW state. The orbital effect establishes the density-wave state. With lowering the temperature the

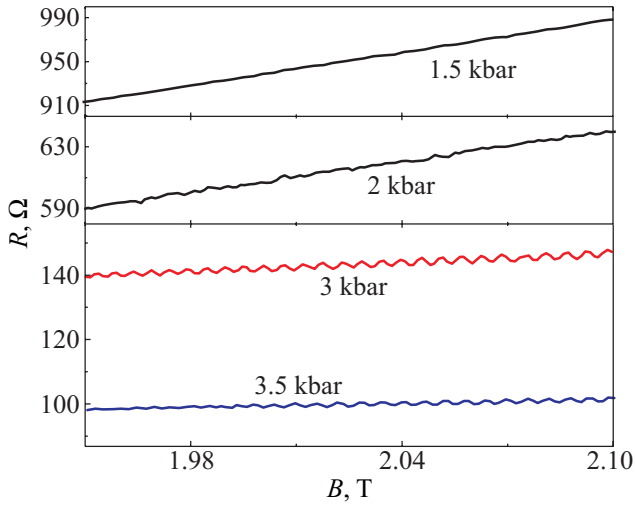

Fig. 2. Low-field part of the curves from Fig. 1 in an enlarged scale. At $P_0 = 2.5$ kbar the fast SdH oscillations start to appear already below 2 T.

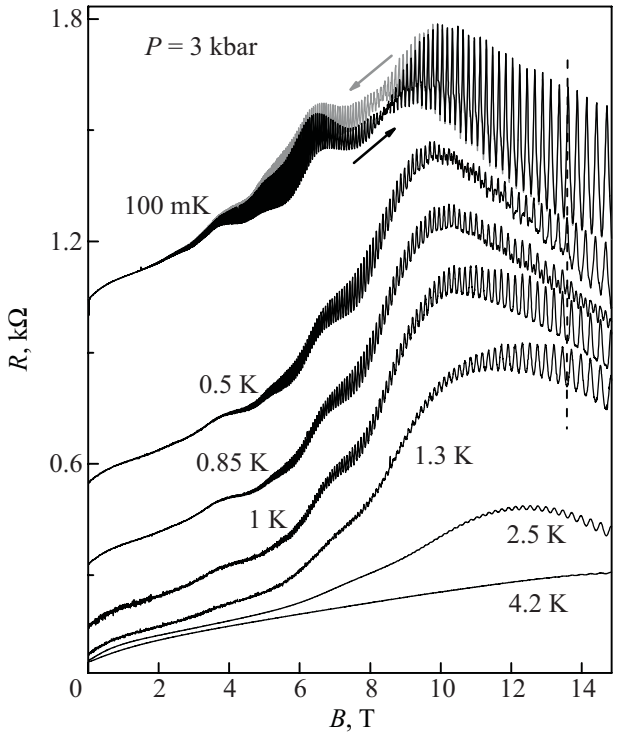

Fig. 3. Magnetoresistance at $P = 3$ kbar. The data are recorded at increasing field and different temperatures. The curves are vertically offset. At the lowest temperature a downward sweep is additionally shown by the grey curve. The vertical dashed line marks a field, at which a minimum in the fast SdH oscillations turns to a maximum upon lowering temperature, which indicates the phase inversion.

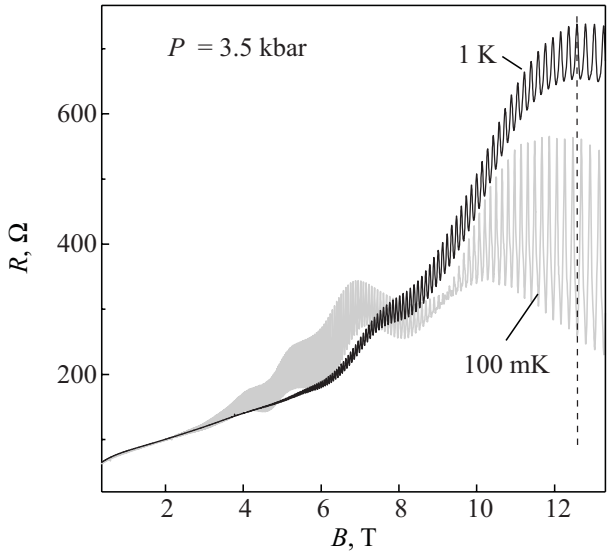

Fig. 4. Magnetoresistance recorded at two different temperatures at $P = 3.5$ kbar. Note the temperature independent resistance at low fields, indicating the normal metallic state. The dashed line at 12.6 T points to the phase inversion.

enhancement of the magnetoresistance shifts to lower fields. Remarkably, the slow oscillations only appear in the field region where the magnetoresistance is elevated. This strongly suggests that the slow oscillations only exist within the re-entrant CDW state.

In the whole temperature range, the slope of the magnetoresistance below 2 T remains approximately the same. Moreover, in this field and pressure region the resistance turns out to be nearly temperature independent as can be seen from Fig. 4, where the field sweeps at 0.1 and 1 K are shown at $P = 3.5$ kbar. This coincides very well with the previous observation that the normal metallic state exists at low fields at $P > P_0 = 2.5$ kbar [15]. The orbits on the Q2D cylindrical Fermi surface are no longer disturbed by the CDW potential, i.e., no magnetic breakdown is required for accomplishing a closed orbit. Hence, it becomes clear why the fast α-oscillations start at such low fields, as shown in Fig. 2.

The presence of the CDW state at higher fields at $P > P_0$ is directly reflected in its distinct properties: First, in the field range of 10–15 T the additional SdH frequencies F_λ and F_ν, characteristic of the CDW state, are observed. An example of the fast Fourier transform (FFT) spectrum of the magnetoresistance at 3.5 kbar is given in Fig. 5. Surprisingly, the frequency F_λ is found to be pressure independent, unlike F_α which in our studies shows a pressure dependence of 17 T/kbar. Second, there is a broad hysteresis in the magnetoresistance between up- and downward sweeps of the magnetic field at $B \geq 3$ T. In Fig. 3 up and down sweeps of the magnetic field are plotted for the lowest temperature, where the broad hysteresis is clearly seen. Such a hysteresis is definitely inconsistent with a normal metallic behavior. On the other hand, it is known to be present in the CDW state of this compound [34–36]. Third, on lowering the temperature a strong decrease of the magnetoresistance background is observed at $B \geq 8$ T, as can be seen in Fig. 4. This is accompanied by a phase inversion of the fast α-oscillations as marked in Figs. 3 and 4 for 3 and 3.5 kbar, respectively, by vertical dashed lines. Such a behavior has already been found to

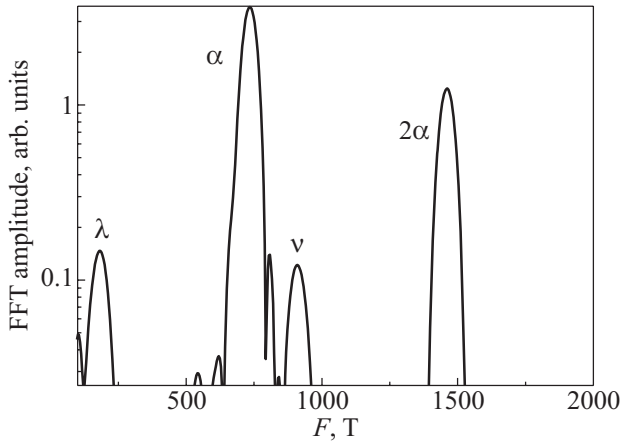

Fig. 5. FFT spectrum of the magnetoresistance at $T = 100$ mK and $P = 3.5$ kbar in the field interval 10–15 T. Peaks corresponding to the additional frequencies F_λ and F_ν characteristic of the re-entrant CDW state are clearly resolved.

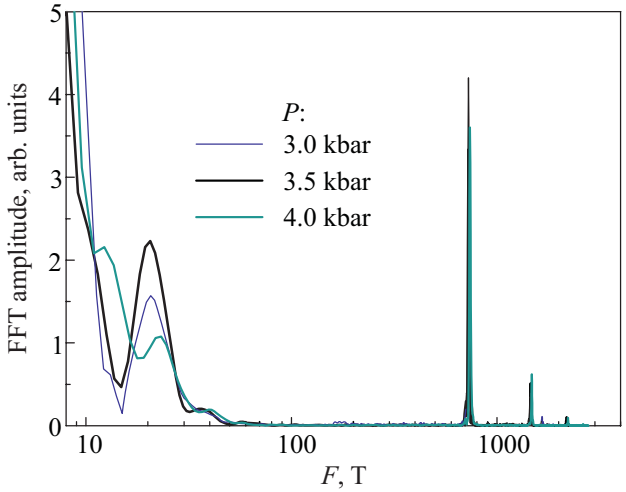

Fig. 6. FFT spectrum in the entire field range, 2–15 T. The additional peak at ≈ 20 T originates from the slow oscillations.

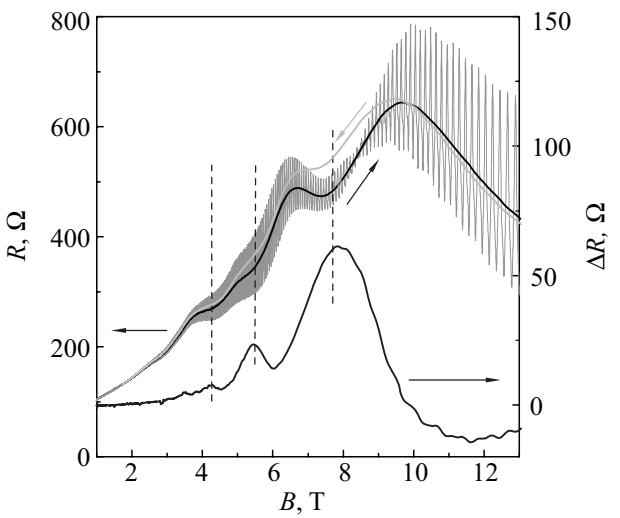

Fig. 7. Field-dependent magnetoresistance background R_{bg} obtained from up- and downward field sweeps by filtering out the SdH oscillatory component (left side scale), the raw data for the upward sweep is shown by the dotted line; P = 3 kbar; T = 100 mK. The hysteresis determined by subtracting one curve from the other (right side scale). Vertical dashed lines are guides to the eye, pointing to a correlation between the anticipated FICDW transition positions (see text) and the structure of the hysteresis.

occur deep in the CDW state and was discussed in a number of publications [21,37–39].

Altogether, the reentrance to the CDW state in magnetic field at pressures between 2.5 and 4 kbar is clearly manifest in the magnetoresistance data. The measured phase transition fields and temperatures are qualitatively well described by the theoretical B–T phase diagrams of a Q1D CDW system at different nesting conditions, which were proposed by Zanchi et al. [19].

Now we turn to the origin of the slow oscillations which exist only in the re-entrant CDW state. At first glance one can suppose that these are SdH oscillations emerging due to small pockets on the Fermi surface, induced by imperfect nesting. This would give a SdH signal of a very low frequency in $1/B$ scale. Indeed, a FFT spectrum in the whole inverse-field range within the re-entrant CDW state shows a peak at about 20 T. The spectra of the oscillations given in Fig. 1 are shown in Fig. 6. Since these peaks are deduced from only very few oscillation periods it is hard to judge about their exact positions. Moreover, since the magnetoresistance background in the CDW state is not known and was evaluated by a low order polynomial fit, an artificial shift of the peak positions ≤ 1 T might arise in the FFT spectrum. We, therefore, cannot judge about the pressure dependence of the low frequency. Nevertheless, a periodicity of these oscillations in $1/B$ is clearly reflected. However, as will be pointed out below, there are several observations which are inconsistent with the standard SdH oscillation behavior and favor the existence of FICDW transitions.

4. FICDW transitions at a perpendicular field

Figure 7 shows the field-dependent magnetoresistance background $R_{bg}(B)$ obtained by filtering out the fast SdH oscillations from the raw $R(B)$ data taken at an up- and downward sweeps of magnetic field (the raw data for the upward sweep is shown by a dotted line), at P = 3 kbar, T = 100 mK. The lower curve in Fig. 7 shows the difference $\Delta R = R^{down}(B) - R^{up}(B)$ between the up- and downsweep traces, demonstrating a considerable hysteresis, which was already mentioned above. The hysteresis exhibits a clear structure correlated with the positions of the slow oscillations: its maxima are located at approximately the field values corresponding to the maximum curvature in $R_{bg}(B)$.

Another feature characteristic of the slow oscillations is a notable temperature dependence of their positions, as illustrated by dashed lines in Fig. 1. This anomalous behavior is certainly not expected for normal SdH oscillations. On the other hand, it is qualitatively quite similar to those observed in the FISDW states of the Bechgaard salts [40,41].

There are further similarities to the FISDW transitions such as, for example, the pressure dependence of the transition fields shown in Fig. 8. The FICDW transition fields were defined from Fig. 1 as the fields of maximum curvature of the magnetoresistance background. Such a choice looks reasonable since these points also correspond to the maxima in the hysteresis structure at 3 kbar. The obtained transition fields at 100 mK move approximately linearly to higher values at increasing pressure. Note that this pressure dependence is quite strong. For SdH oscillations, this would mean a relative expansion of the Fermi surface orbit area at a very high rate, ≈ 0.20 kbar^{-1}. The resulting increase of the SdH frequency must therefore be clearly resolved in the FFT

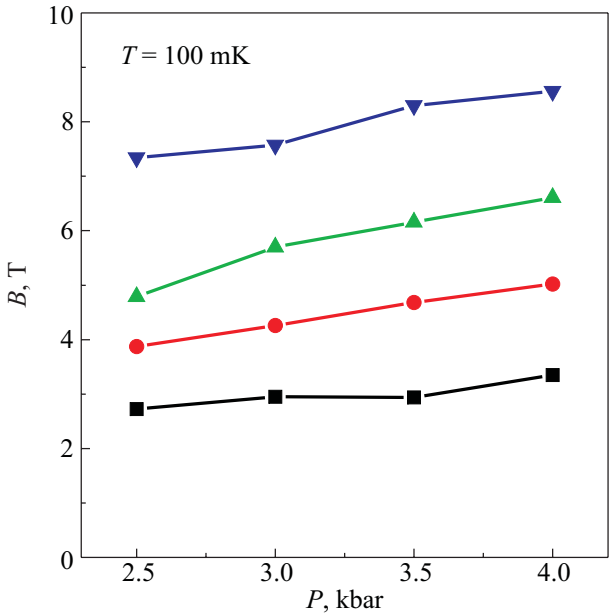

Fig. 8. Pressure dependence of the FICDW transition points (see text) at $T = 100$ mK.

spectrum. Since this is not the case here, this gives another argument against the usual SdH effect as the reason for the observed slow oscillations. On the other hand, the relative positions of the oscillations turn out to be in excellent agreement with the recent generalized FICDW theory [42] based on the electron–phonon interaction concept.

On the whole, we consider these observations as an evidence of first order transitions between subsequent FICDW subphases with quantized wave vectors. Unlike sharp, well defined FISDW transitions found on the Bechgaard salt $(TMTSF)_2PF_6$ [41], the transitions in the present compound as well as the peaks in the hysteresis are rather smeared. A clear hysteresis appears only at temperatures as low as ~ 0.1 K, indicating that well defined first order FICDW transitions occur at considerably lower temperatures than FISDW. This relative weakness of the FICDW instability is caused by the influence of the paramagnetic Pauli effect of magnetic field [20]. Unlike the SDW case, the CDW interaction couples states within the same spin band [43,44]. This effectively causes the paramagnetic suppression of the CDW at high fields [19,45–47] and also has to be taken into account in the FICDW regime. As a matter of fact, the quantization condition for the FICDW wave vector must be extended by an additional Zeeman or Pauli term [20]:

$$Q_x = 2k_F + q_{x,\text{orbital}} \pm q_{x,\text{Pauli}} = 2k_F + NG \pm \frac{2\mu_B B}{\hbar v_F}, \qquad (1)$$

where

$$G = \frac{2ea_c B_z}{\hbar} \quad \text{and} \quad N = 0, \pm 1, \pm 2, ..., \qquad (2)$$

Q_x is the wave vector component in the conducting chain direction, k_F is the Fermi wave vector, μ_B is the Bohr magneton, v_F is the Fermi velocity of the Q1D part of the electron system, a_c is the lattice parameter perpendicular to the conducting chains within the layer, and B_z is the field component perpendicular to the conducting planes. The right hand side of Eq. (1) represents two sets of quantized levels, one for each spin subband. If the quantized values for both spin bands do not match each other, the effective CDW coupling constant decreases, and so does the transition temperature of the FICDW state, as well as the onset temperature of the first order transitions [20].

Finally, we note that a modulation of the SdH oscillation amplitude of the α-frequency in the FICDW states is observed at the lowest temperature (see Fig. 1). Its nature, however, is unclear at present. No direct correlation between the modulation and the FICDW transitions has been found so far. Further measurements are needed to draw any reliable conclusions.

As mentioned above, a mismatch of the quantized levels for different spin bands leads to a decrease of the onset temperature of the first order FICDW transitions. As we will show next there is a possibility to enhance the density wave instability, by changing the magnetic field orientation.

5. FICDW transitions at tilted magnetic fields

While the Zeeman splitting of conduction electrons can be considered as an isotropic effect, the orbital effect essentially depends on the field orientation. In particular, the orbital quantization in this layered material is determined by only the out-of-plane component of magnetic field, $B_z = B \cos\theta$, where θ is the angle between the direction normal to conducting layers and the field direction. On tilting the field the quantized values of each spin subband of the FICDW wave vector given by Eqs. (1), (2) move closer to each other, whereas the distance between the $N = 0$ levels of different subbands, $4\mu_B B/\hbar v_F$, remains the same. Therefore, at certain angles θ the orbital quantization becomes commensurate with the Zeeman splitting and one expects the quantized spin-up levels to coincide with the spin-down ones. For such *commensurate splitting* (CS) angles the FICDW is predicted to become stabilized at higher temperatures [20,48].

In Fig. 9 the field-dependent resistance at $P = 2.8$ kbar is plotted as a function of the out-of-plane field component for different angles, covering an angular range 0–74°. Obviously, the amplitude of the slow oscillations strongly depends on θ. In the shown angle interval there are two regions, around 57° and 71°, where the amplitude of the slow oscillations is maximum, whereas around 43° and 65°, it nearly vanishes. In addition to this angular modulation of the amplitude, the positions of the oscillations also depend on θ : on passing through the angle where the am-

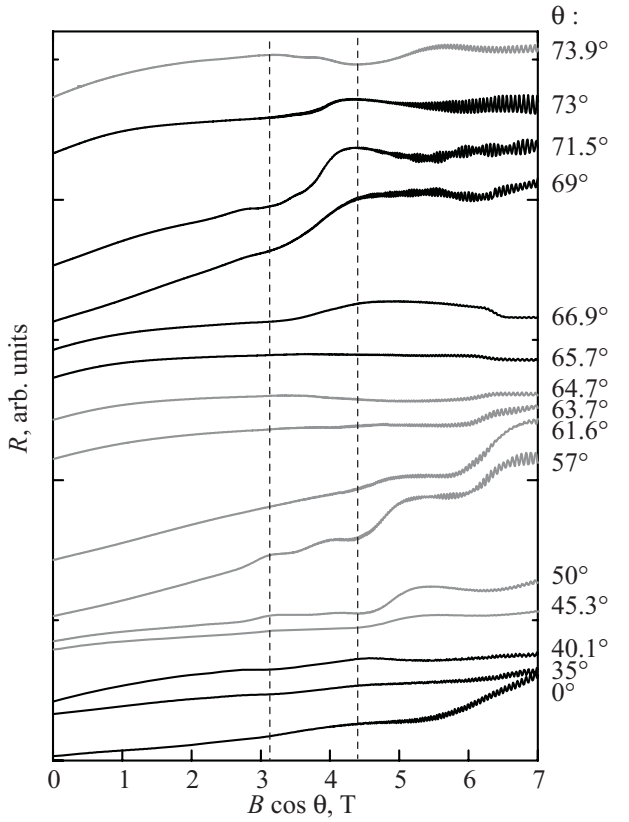

Fig. 9. Magnetoresistance measured at different tilt angles plotted as a function of the out-of-plane field component $B_z = B \cos\theta$, at $T = 0.4$ K, $P = 2.8$ kbar. The curves are offset for clarity. To illustrate the presence of the "spin zeros" effect, vertical dashed lines are drawn through two extrema in the slow oscillations. One can see that at increasing θ the oscillations invert their phase several times.

plitude nearly vanishes, the oscillations shift by half a period. The dashed lines in Fig. 9 mark the transition fields, defined as points of the maximum curvature in the oscillations. One can see that the transition fields change several times their positions on tilting the magnetic field. Thus, the slow oscillations are found to possess a kind of "spin zeros" at certain field directions, similar to what is known for the normal SdH effect in a Q2D metal. In the latter case the phase of the oscillations inverts several times at tilting the magnetic field [49,50].

To understand this behavior of field-induced CDW transitions, we first have to recall in a qualitative manner what happens in a SDW system. At pressures corresponding to FISDW transitions, the x component of the density-wave wave vector also has preferable, quantized values. The spin susceptibility or response function $\chi(Q_x)$ of the system therefore is a quasi-periodic function with maxima at such values of the nesting vector [4]. At not too low temperatures this response, expanded into a harmonic series, is strongly dominated by its first harmonic [51,52]. The same should be true for the present CDW system; however, one has to consider additionally the Zeeman splitting of the spin subbands. The latter can be taken into account by including the spin factor similar to that in the case of the SdH effect:

$$R_S = \cos\left(2\pi\frac{\mu_B B}{\hbar\omega_c}\right) = \cos\left(2\pi\frac{\mu_B}{ea_c v_F\cos\theta}\right), \qquad (3)$$

in the total CDW response function, where $\omega_c = ea_c v_F B\cos\theta/\hbar$ is a characteristic frequency of the orbital motion on the open Fermi surface.

It follows from Eq. (3) that R_S is independent of the magnetic field strength, however, it is sensitive to the sample orientation. In particular, it vanishes at the angles satisfying the "spin-zero" condition:

$$\cos\theta_{sz} = \left(\frac{1}{M+1/2}\right)\frac{2\mu_B}{v_F ea_c}, \qquad (4)$$

where M is an integer. One can easily see that the angles θ_{sz} correspond to the orientation at which quantized values of the CDW wave vector, Eq. (1), for one of the spin subbands lie exactly in the middle between those of the other spin subband. Passing through a spin-zero angle leads to a change of the sign of R_S and, hence, a phase inversion of the response function. This explains the half-period shift of the FICDW transitions in Fig. 9 occurring at $\theta_{sz} = (42.5 \pm 0.5)°$, $(65 \pm 0.2)°$, $(73.5 \pm 0.2)°$, and (not shown in the figure) $(77.8 \pm 0.2)°$.

Another interesting observation is shown in Fig. 10, in which magnetic field sweeps at $T = 0.45$ K, are plotted against $B\cos\theta$ for different angles in the narrow interval

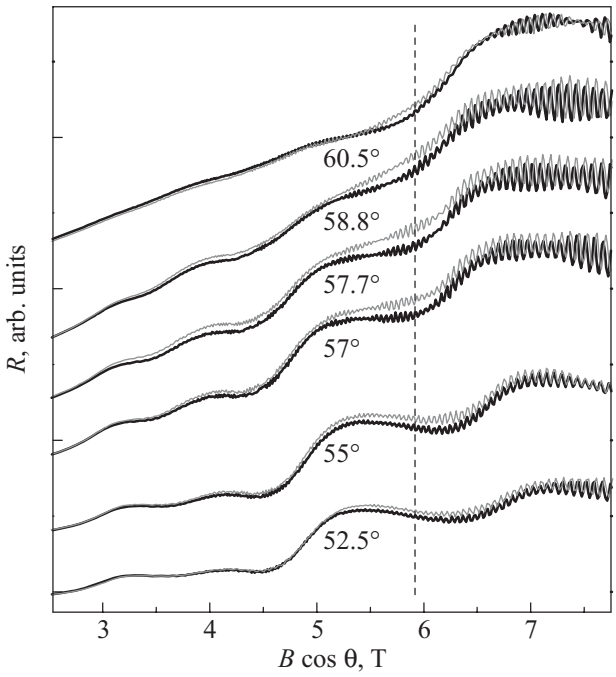

Fig. 10. Detailed view on the up- (black curves) and downward (grey curves) field sweeps of the magnetoresistance in the angular range θ = 52.5 to 60.5°, at $T = 0.45$ K. The position of the vertical dashed line points to the maximum in the hysteresis.

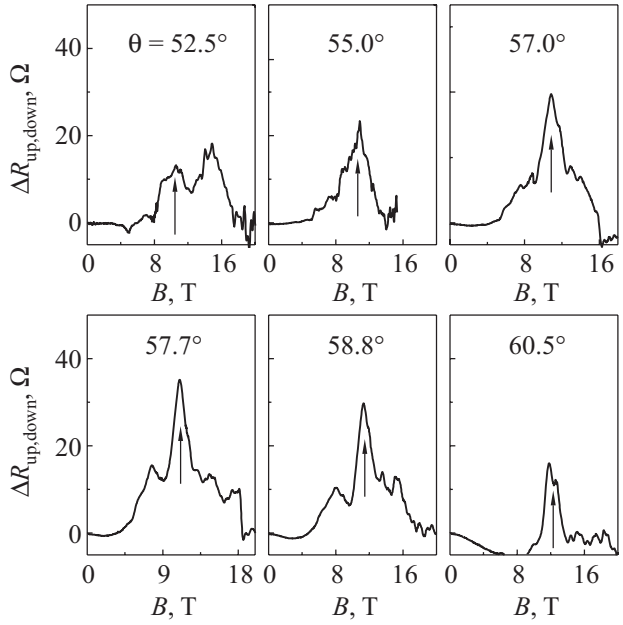

Fig. 11. Hysteresis between up- and downward sweeps of magnetoresistance shown in Fig. 10. The arrow in each panel points to the field having the out-of-plane component $B\cos\theta = 5.9$ T, which corresponds to the position of the vertical dashed line in Fig. 10.

θ = 50–60°. The black curves are taken on sweeping the field up, grey curves on sweeping down. As in the case of the perpendicular field, see Fig. 7, a field-dependent hysteresis between the two sweep directions is observed. This can be directly seen in Fig. 11 showing the magnitude of the hysteresis as a function of field for different θ. Within this angular range the hysteresis becomes strongest at the field-induced transition marked by the vertical dashed line in Fig. 10. Further, it is seen from Fig. 11 that at 57.7° the magnitude of this hysteresis has a maximum. Note that the present temperature is much higher than for the data in Fig. 7; at the perpendicular field orientation no structure in the hysteresis, corresponding to the different FICDW transitions, has been resolved at 0.45 K.

The enhanced magnitude of the hysteretic FICDW features is exactly what one would expect for the CS angles introduced above. Indeed, the angle θ = 57.7° lies in the middle of the interval between two subsequent spin zeros in the inverse cos θ scale. At this orientation the two sets of quantized CDW wave vectors corresponding to different spin subbands coincide with each other, which leads to an increase of the CDW coupling constant and, therefore, to an increase of the FICDW transition temperature.

In the experiment, the angle dependence of the oscillation amplitude around CS angles is rather smooth which makes the determination of θ_{CS} difficult. More precisely can be determined the spin-zero angles at which the oscillations reverse the phase. Figure 12 shows the linear plot of the commensurability index M versus 1/cos θ obtained

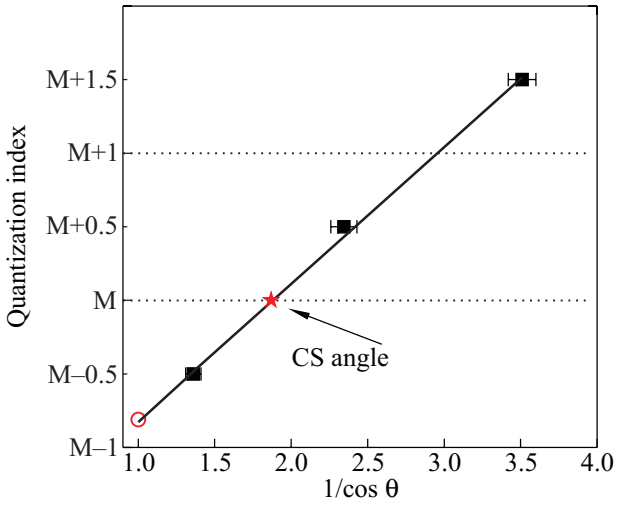

Fig. 12. Positions of the spin-zero angles (see text) plotted according to Eq. (4). Solid line is a linear fit to the experimental data (squares). The star indicates the position of the first CS angle θ = 57.7° and the circle corresponds to the perpendicular field orientation.

from θ_{sz} (squares). The first CS angle, $\theta_{cs} = 57.7°$ (the star symbol in Fig. 12) nicely fits to this plot. As it follows from Eq. (4), the $M(1/\cos\theta)$ dependence can be used for determination of the Fermi velocity on the open Fermi sheets. From our data we obtain $v_F = 1.2\cdot10^5$ m/s.

The circle in Fig. 12 corresponds to the perpendicular field orientation, θ = 0°. One can clearly see that it is situated rather far away from a CS angle value. Therefore, the CDW coupling constant is expected to be considerably suppressed by the paramagnetic effect at this angle. This is why the hysteretic first order FICDW transitions appear at much lower temperatures for this orientation than for CS angles.

6. Angle-dependent magnetoresistance oscillations

The semiclassical component of the interlayer resistance of highly anisotropic metals is known to exhibit oscillations (unrelated to the SdH effect) at rotating a sample in a strong magnetic field. These so-called angle-dependent magnetoresistance oscillations (AMRO) have proved to be a very powerful tool for exploring the Fermi surfaces of organic metals (see, e.g., [53,54] for a review). For α-(BEDT-TTF)$_2$KHg(SCN)$_4$ different kinds of AMRO have been observed depending on experimental conditions.

In the normal metallic state, i.e., at $T > T_{CDW}$ or at $P >> P_0$, the angle-dependent magnetoresistance is dominated by "Q2D" AMRO [55–58]. The latter originates from cyclotron motion of charge carriers on a slightly warped cylindrical Fermi surface [59–63]. Indeed, the Fermi surface of α-(BEDT-TTF)$_2$KHg(SCN)$_4$ accommodates a hole cylinder in addition to the pair of electron open sheets [13,64].

At low temperatures and ambient pressure, i.e., in the CDW state the magnetoresistance is very high at B perpendicular to layers and shows a regular series of sharp dips at tilting the field. The positions of the dips satisfy the so-called Lebed magic angle (LMA) conditions [53,65,66], revealing open trajectories in **k** space. These "Q1D" AMRO are interpreted as a signature of a reconstruction of the cyclotron orbit topology by a CDW potential [28,29,67].

We note that detailed high-pressure AMRO experiments [57,58] were performed at $P \geq 6$ kbar and relatively high temperatures ≥ 1.6 K, which is far above the critical range of suppression of the zero-field CDW state. In this work we have studied the AMRO behavior at a pressure of 2.8 kbar, i.e. just above P_0, in order to reveal the influence of the field-induced CDW. Figure 13 shows $R(\theta)$ curves recorded at different fields in the range 1 to 20 T at T = = 0.7 K. All the curves show prominent AMRO. At high fields they are superposed by fast SdH oscillations which will not be considered here.

At 1 T, the magnetoresistance is minimal at approximately the perpendicular field orientation and shows weak Q2D AMRO. This is consistent with the normal metallic behavior expected for the zero- and low-field state at this pressure. At increasing field, the magnetoresistance rapidly increases at low angles, showing a maximum at $\theta \approx 0°$, and a pair of sharp dips (marked by arrows in Fig. 13) emerges at about ±30°, as one can see from the 4.3, 6.5 and 9 T curves in Fig. 13. Both features strongly resemble the behavior observed at ambient pressure [28,34,35], indicating the field-induced reentrance into a CDW state. However, at higher angles, $|\theta| > 65°$ for $B = 9$ T, the out-of-plane field component reduces below the critical value of a FICDW transition at this temperature and the normal Q2D AMRO pattern is restored. At even higher fields, 15 and 20 T, closed cyclotron orbits reappear due to strong magnetic breakdown, giving rise to Q2D AMRO in the whole angular range. The breakdown is also manifest in enhanced SdH oscillations which are superposed on the semiclassical AMRO. A similar magnetic-breakdown induced crossover from the Q1D AMRO to the Q2D AMRO regime is well known for the ambient-pressure CDW state [30,31].

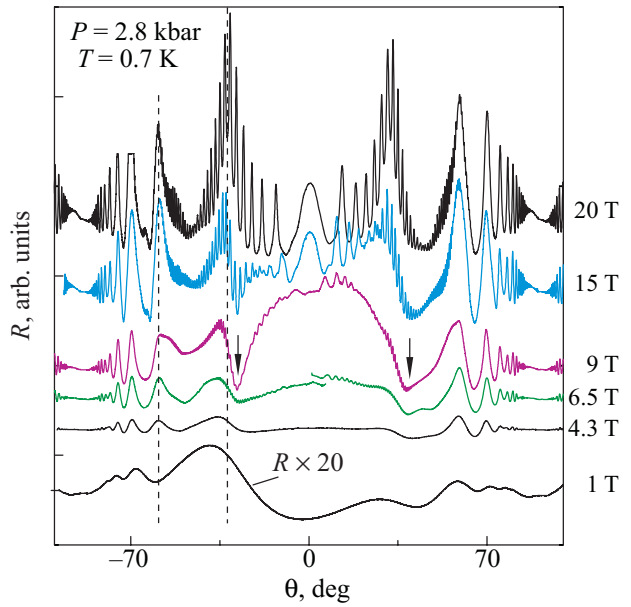

Fig. 13. Angle-dependent magnetoresistance for several different fields at $P = 2.8$ kbar, $T = 0.7$ K. The curves are vertically offset for clarity. The resistance at 1 T is magnified by a factor of 20. The arrows point to the sharp Q1D AMRO dips in the 9 T curve, typical of the CDW state. Dashed lines are drawn at the positions of the high-field Q2D AMRO peaks, revealing their difference from the positions of Q2D AMRO at 1 T.

On the whole, our AMRO data for $P = 2.8$ kbar is fully consistent with the FICDW scenario discussed in the previous sections. Since the hysteretic first order transitions were found to emerge at the CS angles at temperatures higher than in the perpendicular orientation, one could also expect some additional features at these angles. One can indeed resolve an anomalous feature at $\theta \approx 57°$; however, it is too weak to draw an unambiguous conclusion about its origin. This is not very surprising, since the present temperature is relatively high so that the CS angle effect is likely smoothed out.

Finally, we note that the Q2D pattern in the strong magnetic breakdown regime is not exactly the same as at the fields below the FICDW transitions. This is illustrated, for example, by vertical dashed lines in Fig. 13, which are drawn through two subsequent AMRO peaks on the 20 T curve and clearly do not match peak positions on the 1 T curve. One could speculate that the apparent discrepancy is due to a different geometry of cyclotron orbits in the low- and high-field states. On the other hand, one has to take into account that the standard AMRO positions [59–62] derived for the high-field limit may not hold down to $B = 1$ T [63]. More detailed studies, in both high- and low-field ranges are required for clarifying this issue.

7. Conclusion

The presented results provide a firm evidence that the CDW state in α-(BEDT-TTF)$_2$KHg(SCN)$_4$ can be stabilized at pressures above critical by applying magnetic field of ≥ 3 T. At low enough temperatures, the magnetoresistance of this re-entrant CDW phase displays a nonmonotonic behavior and a considerable hysteresis, indicating a cascade of first order FICDW transitions.

Like the well-known FISDW transitions, the FICDW phenomenon is primarily caused by the quantizing orbital effect of a magnetic field. However, by contrast to its spin-density-wave analog, it is sensitive to the Pauli paramagnetic effect. The latter leads to a decrease of the CDW coupling constant [20] and, hence, to a relatively narrow temperature/pressure range in which FICDW transitions can be observed. However, by tilting the field, it is possible

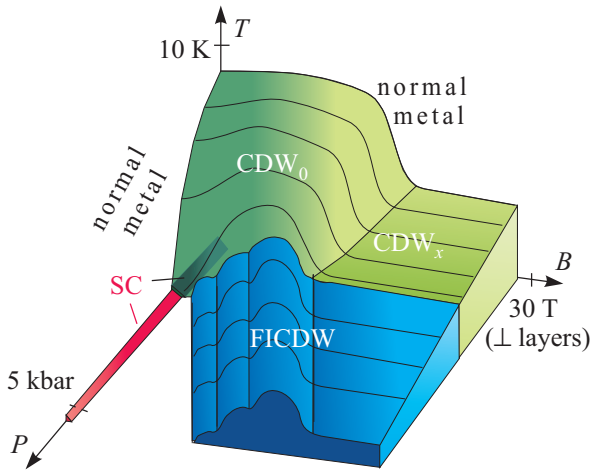

Fig. 14. Schematic phase diagram of α-(BEDT-TTF)$_2$KHg(SCN)$_4$ including the low-field CDW$_0$ and high-field CDW$_x$ states at pressures below $P_0 \approx 2.5$ kbar, the FICDW region above P_0, and a low-temperature superconducting state (SC) coexisting and competing with the density-wave instability.

to tune the orbital quantization, thus achieving commensurability of the orbital and spin splitting effects at certain field orientations.

The variety of electronic states in the present compound is illustrated by the schematic *B*–*T*–*P* phase diagram shown in Fig. 14. In addition to the normal metallic and FICDW regions discussed in this work, it incorporates the low-pressure, low-field CDW$_0$ and low-pressure, high-field CDW$_x$ states [9–11] as well as a low-temperature superconducting state [15]. The rich phase diagram and high crystal quality make this compound an excellent model object for studying the interplay between different instabilities of the normal metallic state caused by low dimensionality and electron interactions.

Acknowledgment

The work was supported in part by the EU Access to Research Infrastructure Action of the Improving Human Potential Programme and by the Federal Agency of Science and Innovations of Russian Federation under Contract No. 14.740.11.0911.

1. T. Ishiguro, K. Yamaji, and G. Saito, *Organic Superconductors*, 2nd edition, Springer-Verlag, Berlin, Heidelberg (1998).
2. *The Physics of Organic Superconductors and Conductors*, A.G. Lebed (ed.), Springer Verlag, Berlin, Heidelberg (2008).
3. L.P. Gor'kov and A.G. Lebed, *J. Phys. (Paris)* **45**, L433 (1984).
4. G. Montambaux, M. Heritier, and P. Lederer, *Phys. Rev. Lett.* **55**, 2078 (1985).
5. P.M. Chaikin, *Phys. Rev.* **B31**, 4770 (1985).
6. A.G. Lebed, *Zh. Eksp. Teor. Fiz.* **89**, 1034 (1985) [*Sov. Phys. JETP* **62**, 595 (1985)].
7. J.F. Kwak, J.E. Schirber, P.M. Chaikin, J.M. Williams, H.-H. Wang, and L.Y. Chiang, *Phys. Rev. Lett.* **56**, 972 (1986).
8. P.M. Chaikin, *J. Phys. I (France)* **6**, 1875 (1996).
9. N. Biskup, J.A.A.J. Perenboom, J.S. Brooks, and J.S. Qualls, *Solid State Commun.* **107**, 503 (1998).
10. P. Christ, W. Biberacher, M.V. Kartsovnik, E. Steep, E. Balthes, H. Weiss, and H. Müller, *Pis'ma Zh. Eksp. Teor. Fiz.* **71**, 437 (2000) [*JETP Lett.* **71**, 303 (2000)].
11. M.V. Kartsovnik, D. Andres, W. Biberacher, P. Christ, E. Steep, E. Balthes, H. Weiss, H. Müller, and N.D. Kushch, *Synth. Met.* **120**, 687 (2001).
12. P. Foury-Leylekian, S. Ravy, J.-P. Pouget, and H. Müller, *Synth. Met.* **137**, 1271 (2003).
13. P. Foury-Leylekian, J.-P. Pouget, Y.-J. Lee, R.M. Nieminen, P. Ordejón, and E. Canadell, *Phys. Rev.* **B82**, 134116 (2010).
14. D. Andres, M.V. Kartsovnik, W. Biberacher, H. Weiss, E. Balthes, H. Müller, and N. Kushch, *Phys. Rev.* **B64**, 161104(R) (2001).
15. D. Andres, M. Kartsovnik, W. Biberacher, K. Neumaier, E. Schuberth, and H. Müller, *Phys. Rev.* **B72**, 174513 (2005).
16. D. Andres, M. Kartsovnik, P.D. Grigoriev, W. Biberacher, and H. Müller, *Phys. Rev.* **B68**, 201101(R) (2003).
17. K. Yamaji, *J. Phys. Soc. Jpn.* **53**, 2189 (1984).
18. A. Bjelis and D. Zanchi, in: *The Physics of Organic Superconductors and Conductors*, A.G. Lebed (ed.), Springer Verlag, Berlin, Heidelberg (2008), p. 589.
19. D. Zanchi, A. Bjelis, and G. Montambaux, *Phys. Rev.* **B53**, 1240 (1996).
20. A.G. Lebed, *Pis'ma Zh. Eksp. Teor. Fiz.* **78**, 170 (2003) [*JETP Lett.* **78**, 138 (2003)].
21. D. Andres, M.V. Kartsovnik, W. Biberacher, T. Togonidze, H. Weiss, E. Balthes, and N. Kushch, *Synth. Met.* **120**, 841 (2001).
22. M.V. Kartsovnik, D. Andres, W. Biberacher, P.D. Grigoriev, E.A. Schuberth, and H. Müller, *J. Phys. IV (France)* **114**, 191 (2004).
23. M.V. Kartsovnik, D. Andres, P.D. Grigoriev, W. Biberacher, and H. Müller, *Physica* **B346–347**, 368 (2004).
24. D. Graf, E.S. Choi, J.S. Brooks, M. Matos, R.T. Henriques, and M. Almeida, *Phys. Rev. Lett.* **93**, 076406 (2004).
25. K. Murata, K. Yokogawa, K. Kobayashi, K. Masuda, T. Sasaki, Y. Seno, N.R. Tamilselvan, H. Yoshino, J.S. Brooks, D. Jerome, K. Bechgaard, M. Uriuchi, K. Yakushi, Y. Nogami, and R. Kato, *J. Phys. Soc. Jpn.* **79**, 103702 (2010).
26. H. Mori, S. Tanaka, K. Oshima, M. Oshima, G. Saito, T. Mori, Y. Maruyama, and H. Inokuchi, *Solid State Commun.* **74**, 1261 (1990).
27. H. Müller and Y. Ueba, *Synthesis* **9**, 853 (1993).
28. M.V. Kartsovnik, A.E. Kovalev, and N.D. Kushch, *J. Phys. I (France)* **3**, 1187 (1993).
29. M.V. Kartsovnik, in: *The Physics of Organic Superconductors and Conductors*, A.G. Lebed (ed.), Springer Verlag, Berlin, Heidelberg (2008), p. 185.

30. R.H. McKenzie, G.J. Athas, J.S. Brooks, R.G. Clark, A.S. Dzurak, R. Newbury, R.P. Starrett, A. Skougarevsky, M. Tokumoto, N. Kinoshita, T. Kinoshita, and Y. Tanaka, *Phys. Rev.* **B54**, 8289(R) (1996).
31. A. House, C.J. Hawoth, J.M. Caulfield, S. Blundell, M.M. Honold, J. Singleton, W. Hayes, S.M. Hayden, P.J. Meeson, M. Springford, M. Kurmoo, and P. Day, *J. Phys.: Condens. Matter* **8**, 10361 (1996).
32. N. Harrison, E. Rzepniewski, J. Singleton, P.J. Gee, M.M. Honold, P. Day, and M. Kurmoo, *J. Phys.: Condens. Matter* **11**, 7227 (1999).
33. N. Harrison, N. Biskup, J.S. Brooks, L. Balicas, and M. Tokumoto, *Phys. Rev.* **B63**, 195102 (2001).
34. T. Osada, R. Vagi, A. Kawasumi, S. Kagoshima, N. Miura, M. Oshima, and G. Saito, *Phys. Rev.* **B41**, 5428 (1990).
35. T. Sasaki and N. Toyota, *Solid State Commun*. **82**, 447 (1993).
36. M.V. Kartsovnik, D.V. Mashovets, D.V. Smirnov, V.N. Laukhin, A. Gilewski, and N.D. Kushch, *J. Phys. I (France)* **4**, 159 (1994).
37. M.V. Kartsovnik, W. Biberacher, E. Steep, P. Christ, K. Andres, A.G.M. Jansen, and H. Müller, *Synth. Met.* **86**, 1933 (1997).
38. M. Honold, N. Harrison, J. Singleton, M.-S. Nam, S.J. Blundell, C.H. Mielke, M. Kartsovnik, and N. Kushch, *Phys. Rev.* **B59**, 10417(R) (1999).
39. N. Harrison, L. Balicas, J.S. Brooks, and M. Tokumoto, *Phys. Rev.* **B62**, 14212 (2000).
40. K. Kajimura, H. Tokumoto, M. Tokumoto, K. Murata, T. Ukachi, H. Anzai, T. Ishiguro, and G. Saito, *J. Phys. (France)* **44**, 1059 (1983).
41. A.V. Kornilov, V.M. Pudalov, Y. Kitaoka, K. Ishida, T. Mito, J.S. Brooks, J.S. Qualls, J.A.A.J. Perenboom, N. Tateiwa, and T.C. Kobayashi, *Phys. Rev.* **B65**, 060404(R) (2002).
42. A.G. Lebed, *Phys. Rev. Lett.* **103**, 046401 (2009).
43. J. Sólyom, *Adv. Phys.* **28**, 201 (1979).
44. G. Grüner, *Density Waves in Solids*, Addison Wesley (1994).
45. P. Fulde and R.A. Ferrell, *Phys. Rev*. **135**, A550 (1964).
46. A.I. Buzdin and V.V. Tugushev, *Zh. Eksp. Teor. Fiz.* **85**, 735 (1983) [*Sov. Phys. JETP* **58**, 428 (1983)].
47. P.D. Grigoriev and D.S. Lyubshin, *Phys. Rev.* **B72**, 195106 (2005).
48. A. Bjelis, D. Zanchi, and G. Montambaux, *J. Phys. IV (France)* **9**, PR10 (1999).
49. D. Shoenberg, *Magnetic Oscillations in Metals*, Cambridge University Press, Cambridge (1984).
50. J. Wosnitza, *Fermi Surfaces of Low-Dimensional Organic Metals and Superconductors*, Springer-Verlag, Berlin, Heidelberg (1996).
51. A.G. Lebed, *Phys. Rev. Lett.* **88**, 177001 (2002).
52. A.G. Lebed, *Pis'ma Zh. Eksp. Teor. Fiz.* **72**, 205 (2000) [*JETP Lett.* **72**, 141 (2000)].
53. M.V. Kartsovnik, *Chem. Rev.* **104**, 5737 (2004).
54. M.V. Kartsovnik and V.G. Peschansky, *Fiz. Nizk. Temp*. **31**, 249 (2005) [*Low Temp. Phys*. **31**, 185 (2005)].
55. A.E. Kovalev, M.V. Kartsovnik, R.P. Shibaeva, L.P. Rozenberg, I.F. Schegolev, and N.D. Kushch, *Solid State Commun*. **89**, 575 (1994).
56. M.V. Kartsovnik, A.E. Kovalev, V.N. Laukhin, I.F. Schegolev, H. Ito, T. Ishiguro, N.D. Kushch, H. Mori, and G. Saito, *Synth. Met.* **70**, 811 (1995).
57. N. Hanasaki, S. Kagoshima, N. Miura, and G. Saito, *J. Phys. Soc. Jpn*. **65**, 1010 (1996).
58. N. Hanasaki, S. Kagoshima, N. Miura, and G. Saito, *Phys. Rev.* **B63**, 245116 (2001).
59. K. Yamaji, *J. Phys. Soc. Jpn.* **58**, 1520 (1989).
60. V.G. Peschansky, J.A. Roldan Lopez, and Toji Gnado Yao, *J. Phys. I (France)* **1**, 1469 (1991).
61. R. Yagi, Y. Iye, T. Osada, and S. Kagoshima, *J. Phys. Soc. Jpn.* **59**, 3069 (1990).
62. M.V. Kartsovnik, V.N. Laukhin, S.I. Pesotskii, I.F. Shchegolev, and V.M. Yakovenko, *J. Phys. I (France)* **2**, 89 (1992).
63. P.D. Grigoriev, *Phys. Rev.* **B81**, 205122 (2010).
64. H. Mori, S. Tanaka, M. Oshima, G. Saito, T. Mori, Y. Maruyama, and H. Inokuchi, *Bull. Chem. Soc. Jpn.* **63**, 2183 (1990).
65. A.G. Lebed, *Pis'ma Zh. Eksp. Teor. Fiz.* **43**, 137 (1986) [*JETP Lett.* **43**, 174 (1986)].
66. S. Wu and A.G. Lebed, *Phys. Rev.* **B82**, 075123 (2010).
67. M.V. Kartsovnik, A.E. Kovalev, V.N. Laukhin, and S.I. Pesotskii, *J. Phys. I (France)* **2**, 223 (1992).